IOP Publishing Superconductor Science and Technology
Supercond. Sci. Technol. 31 (2018) 085003 (8pp) https://doi.org/10.1088/1361-6668/aac871

Lightweight MgB_2 wires with a high temperature aluminum sheath made of variable purity Al powder and Al_2O_3 content

P Kováč[1], I Hušek[1], M Kulich[1], J Kováč[1], T Melišek[1], L Kopera[1], N Perez[2], W Haessler[2], M Balog[3], P Krížik[3] and D Berek[1]

[1] Institute of Electrical Engineering, Slovak Academy of Sciences, Dúbravska cesta 9, 841 04 Bratislava, Slovakia
[2] Leibniz-Institute for Solid State and Materials Research (IFW), D-01171 Dresden, Germany
[3] Institute of Materials and Machine Mechanics, Slovak Academy of Sciences, Dúbravska cesta 9, 84513 Bratislava, Slovakia

E-mail: Pavol.Kovac@savba.sk

Received 16 April 2018, revised 17 May 2018
Accepted for publication 29 May 2018
Published 25 June 2018

Abstract

The properties of high temperature aluminum (HITEMAL, hereinafter HIT) composites made of powders with different particle sizes ranging from 0.8–3 μm and purities of 99.9%–99.996% were tested. The thermal, electrical, and mechanical properties of these materials were examined and compared with pure Al. Three different HIT materials were used for the outer sheath of single-core MgB_2 wires with a Ti barrier manufactured by internal magnesium diffusion into a boron process. The critical currents, thermal stability, and strain tolerances of the MgB_2/Ti/HIT wires were measured at liquid He temperature. It was found that the Al powder purity and particle size used for HIT affect the performance of MgB_2 wires. A sheath made of high purity Al powder allows better thermal stability of MgB_2 wire, but the strain tolerance is lower in comparison to the wire with HIT made of less pure powder and higher Al_2O_3 content. The presented wire configurations are promising for lightweight, thermally stabile, and strain tolerant superconducting MgB_2 wires.

Keywords: MgB_2, light MgB_2/Ti/Al wire, Al-Al_2O_3 composite, thermal conductivity, critical currents, strain tolerance

(Some figures may appear in colour only in the online journal)

1. Introduction

Metallic sheaths play an important role in and considerably affect the performance of superconducting filaments, especially if they is manufactured by a powder-in-tube (PIT) process [1–4]. The main requirements for an outer sheath are: (i) good formability by drawing or rolling with high wire size reduction ($d_{initial}/d_{final} > 25$), preferably without intermediate annealing, (ii) high thermal and electrical conductivity, and (iii) high mechanical strength in the final stage (after the final heat treatment). In addition, any chemical reaction of metallic sheath with MgB_2 filaments is undesirable and has to be protected by inert barrier material. Until now, several metallic materials have been used for the outer sheath of MgB_2 wires made by PIT: Cu, Ni, Monel, GlidCop, and stainless steel [5–9]. The stronger the outer sheath, the higher the density the MgB powder mixture is and consequently, denser MgB_2 filaments are created during the final heat treatment [10]. But MgB_2 filaments made by the PIT process still have high porosity, which limits the transport current density. The magnesium infiltration process introduced by Giunchi *et al* [11, 12] uses B powder around a central metallic Mg-core that allows the creation of a very dense MgB_2 phase and, consequently, high current densities—as already presented by several laboratories using this so-called 'internal magnesium diffusion (IMD) process' [13–17]. Reaching the high engineering current density of MgB_2 wires made by IMD is very important for future exploitation in practical applications of

Table 1. The main characteristics of gas atomized Al powders B, C, and D in comparison to pure metallic aluminum A.

Sample	A	B	C	D
Purity (%)	99.999	99.995	99.9	99.9
Al_2O_3 (vol %)	0	1.6	1.5	3.1
d_{50} (μm)	—	1.9	3.0	0.8

this superconductor in superconducting systems. For some superconducting applications [18–21], low total mass of the system is also an important issue. Therefore, the idea of using thermal stabilization of the MgB_2 wire with a lightweight Al-based outer sheath is interesting. Al-Al_2O_3 composites formed *in situ* during the consolidation of ultrafine Al powders have been developed for mechanical components [22]. Cold deformation of as-extruded Al-Al_2O_3 rods has been initially tested by rolling and drawing into a wire and the wire's properties were measured at low temperatures [23]. The first MgB_2 wire with Ta barrier and Al-Al_2O_3 sheath was successfully made by an IMD process [24]. It has already been shown that the combination of the MgB_2 phase (2.5 gcm^{-3}) with a Ti barrier (4.5 gcm^{-3}) and a light Al-Al_2O_3 outer sheath (~2.7 gcm^{-3}) into composite wire provides a superconductor with the minimum possible mass [25].

This work presents the basic properties of three different Al + Al_2O_3 sheath materials and single-core MgB_2/Ti/Al–Al_2O_3 wires manufactured by the IMD process to demonstrate the effect of applied Al–Al_2O_3 sheaths to the electrical, thermal, and mechanical properties of wires.

2. Experimental

2.1. HITEMAL wires

Three different *in situ* Al–Al_2O_3 metal matrix composites (called HITEMAL, hereinafter HIT) have been fabricated by a powder metallurgy approach using aluminum powders [22] of different purities ranging from 99.9%–99.999% and particle sizes 0.8–3.0 μm. Gas atomized Al powders B, C, and D (see table 1) were pressed by a cold isostatic pressure of 200 MPa and subjected to vacuum degassing prior to uniaxial vacuum hot pressing. Direct extrusion was made with a reduction ratio of ~7:1 at 425 °C using a die with a diameter of 13 mm. Then, groove rolling and rotatory swaging deformations were applied at room temperature down to an ~1.1 mm wire diameter without any intermediate annealing [23]. The properties of the pure metallic wire Al (wA) and three HIT compositions wB, wC, and wD were tested thermally, electrically, and mechanically.

Thermal conductivity measurements of the short samples were performed in the Physical Property Measurement System Dynacool from Quantum Design equipped with the latest available version of the Thermal Transport Option. Four Au coated Cu contacts were attached to the cut wires using Ag filled epoxy H20C from EPO-TEK. Thermal conductivity data were determined while ramping the temperature of the sample chamber from 300–1.8 K at a rate of 0.3 K min^{-1}. Heat pulses were continuously applied to one end of the sample. The heat conductivity was obtained by fitting the time dependent temperature difference between the hot and cold ends of the sample. Electrical resistivity of the wires (wA–wD) was measured by a standard four-probe method between 25 and 300 K with a DC magnitude of 100 mA. Differential scanning calorimetry (DSC) thermal analysis of the wires AD was done in argon atmosphere at the temperature range of 540 °C–730 °C using a NETZSCH DSC instrument. The ramping of temperature was 1.5 K min^{-1} with the measured temperature repeatability of ±0.1 °C. The mechanical properties of the as-deformed (AD) and heat treated (HT) wires were tested by axial tension at room temperature and also at 77 K.

2.2. MgB_2/Ti/HIT wires

As-extruded HIT rods were rotary swaged from 13–11 mm and then 8 mm holes were drilled. Subsequent swaging on the hardened mandrel allows us to make 6.2/9.0 mm tubes from compositions B, C, and D which were used for the outer sheath of the composite MgB_2 wires. Single-core MgB_2 wires were composed of pure Mg wire of 2.9 mm in diameter surrounded by boron powder (purity 99.8%, <1 μm, filled in a glove-box) inside the 5.5/7.0 mm Ti tube. The Mg/B/Ti composite was rotary swaged down to 6.0 mm and inserted into the HIT tubes B, C, and D with an inner/outer diameter of 6.2/9.0 mm, swaged to 7.5 mm and then groove rolled into a rectangular composite wire of size 1.14 × 1.14 mm named rwB, rwC, and rwD. Short pieces of rectangular 1.7 × 1.7 mm rolled wires were also deformed by rotary swaging down to 1.14 mm in diameter with a 20% reduction per pass at IFW Dresden (named swB, swC, and swD). Intermediate heat treatment at 450 °C/30 min was applied after a 60%–70% area reduction under argon atmosphere. The Mg/B/Ti/HIT wires were finally HT under argon atmosphere at a temperature of 635 °C for 15 min (for swaged) and 640 °C/60 min (for rolled wires). Optical microscopy with an Olympus GX 51 was used for the characterization of wires cross-sections and interface reactions. Nanoindentation measurements across the MgB_2/Ti/HIT interfaces were performed using a Hysitron TI 750 Ubi machine with a peak force of 7 N and a dwell time of 2 s. The microhardness measurements were conducted using 0.5 kp force and 10 s indentation time using a Future-Tech FM-ARS 9000 indenter. Transport critical currents were measured at liquid He temperature and an external magnetic field between 4.0 and 8.0 T using a standard DC measurement with 1 μV cm^{-1} criterion. To quantify the thermal stability of the presented wires, *I*–*V* characteristics with the constant current ramping 0.43 As^{-1} above the I_c criterion were measured and the quench power of the rolled and swaged wires evaluated and compared. The electro-mechanical characteristics: I_c versus the tensile strain (ε) and the stress–strain curves $\sigma(\varepsilon)$ were measured at a constant external magnetic field of 6 T.

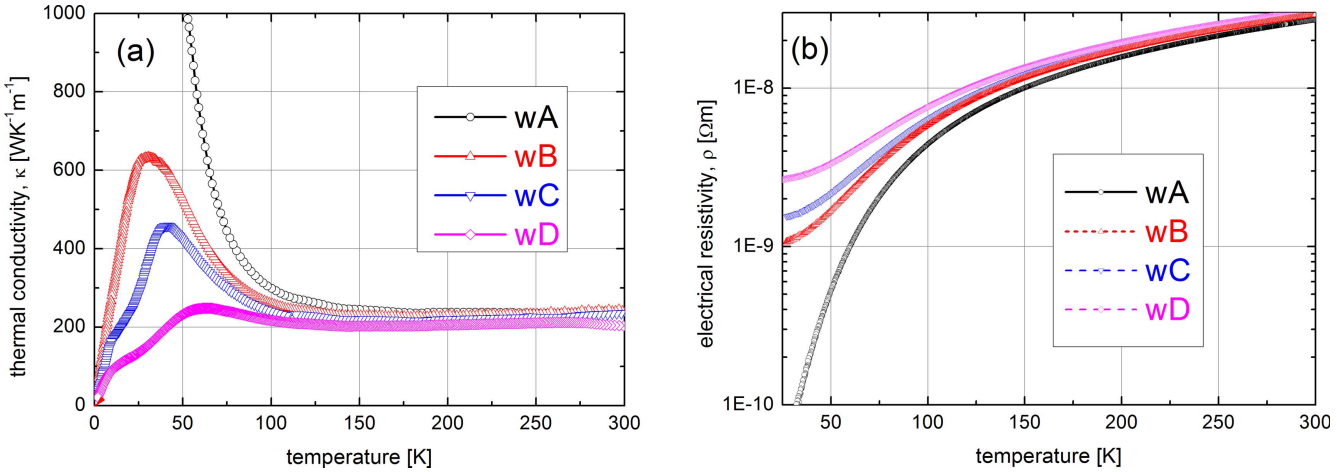

Figure 1. Thermal conductivities of pure Al (wA) and HIT wires wB–wD between 300 and 1.8 K (a) and electrical resistivity of these wires between 300 and 25 K (b).

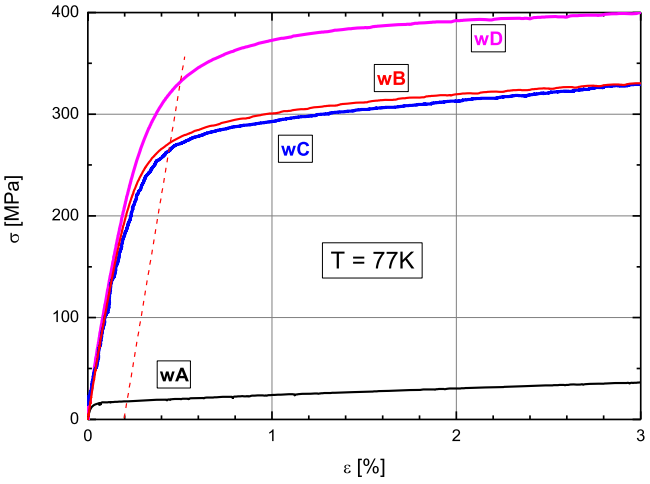

Figure 2. Stress–strain ($\sigma(\varepsilon)$) characteristics of wires wA–wD measured at 77 K. The dashed line shows the 0.2% strain offset stress ($YS_{0.2}$) of the compared wires at crossing with individual $\sigma(\varepsilon)$.

Table 2. Selected low temperature properties of compared Al wire wA with HIT wires wB–wD: thermal conductivity at 50 K, resistivity at 50 K, and 0.2% strain offset stress ($YS_{0.2}$) at 77 K.

Parameter	wA	wB	wC	wD
$\kappa_{(50K)}$ ($WK^{-1}m^{-1}$)	1100	524	427	233
$\rho_{(50K)}$ (10^{-9} Ωm)	0.54	1.66	2.15	3.37
$YS_{0.2(77K)}$ (MPa)	20	272	263	322

3. Results and discussion

3.1. Properties of HIT wires

Figure 1 shows the temperature dependences of the thermal conductivity (κ) and electrical resistivity (ρ) of the four examined wires. One can see the relation between κ and ρ, which is given by the Wiedemann–Franz law stating that the ratio of κ/σ ($\sigma = 1/\rho$) of metals is proportional to its temperature. The thermal conductivity of Al–Al_2O_3 is, like electrical resistivity, determined largely by the free electrons and directly proportional to the mean free path affected by Al powder purity and Al_2O_3 content, see table 2. It is evident that the purity of Al affects the values of κ and ρ considerably, especially at temperatures below 40 K, where a MgB_2 superconductor can be utilized. Consequently, the selection of Al powder for the HIT material aimed for thermal stabilization of superconducting wire is important and high κ and low ρ are preferred. But, as mentioned above, the mechanical properties have to also be considered. Figure 2 shows the stress–strain characteristics obtained at 77 K for the HIT wires in comparison to the pure Al wire. The 0.2% strain offset stress $YS_{0.2}$ (77 K) of all wires is compared in table 2, where more than a one order of magnitude increase of $YS_{0.2}$ is clearly demonstrated for the wB–wD wires in comparison to the pure Al. Table 2 shows that wire wB is a promising material for possible applications due to considerably increased $YS_{0.2(77K)}$ and less affected $\kappa_{(50K)}$ and $\rho_{(50K)}$ in comparison to pure Al.

Due to the necessity of heat treatment of superconducting wires with the HIT sheath close to the melting temperature of magnesium (650 °C), DSC was applied for the wA–wD wires. The result of the DSC experiment is a curve of heat flux versus temperature and measures the amount of energy absorbed or released by a sample when it is heated or cooled, providing quantitative and qualitative data on endothermic and exothermic processes and an estimate of the melting temperature. Figure 3 shows the DSC curves of the compared wires between 640 °C and 720 °C. A DSC trace of melting of pure Al showing a typical single peak due to melting of the Al rich phase at 660 °C is depicted in figure 3 for wA and wB. The DCS trace of wB is similar, but the melting point of Al is shifted to lower temperature $T_m \sim 658$ °C. Wires wC and wD have different slopes in comparison to wA with a more flat 'melting' area (650 °C–660 °C, $T_m < 653$ °C) and the peaks are lowered by 11.5%. These characteristics show that the melting temperature slowly decreases with the increase in the content of Al_2O_3, which is important to know for the final heat treatment of MgB_2 wires close to 650 °C. The effect of the final heat treatment on the mechanical properties of the

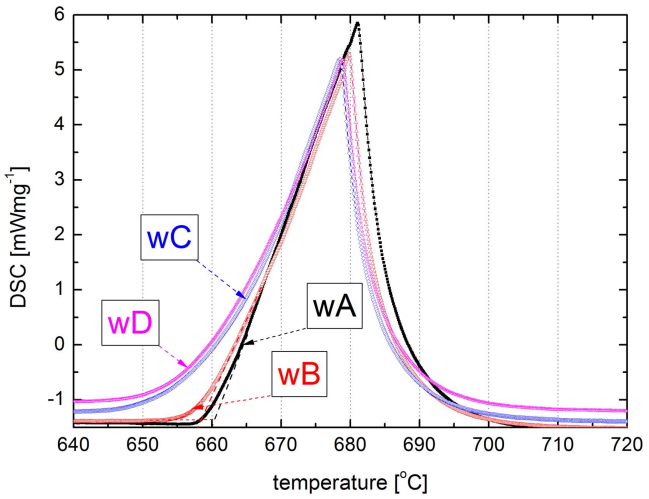

Figure 3. DCS traces of HIT wires wA–wD between 640 °C and 720 °C.

HIT has been verified for the temperature profiles suitable for the fast creation of dense MgB_2 by the IMD process [26]. Figure 4(a) shows the three heat treatment profiles applied for wire wB with the temperature overheating by 19 K due to fast ramping up ($\sim$100 °C min^{-1}). Figure 4(b) presents the corresponding stress–strain curves measured at room temperature compared with the AD wire. One can see a considerable softening of the outer sheet if the maximal temperature during the heat treatment reaches only shortly the melting point $\sim$658 °C. Only heat treatment at 632 °C/10 min with the peak temperature of 651 °C allows the stressing of the wB wire above 100 MPa.

3.2. Properties of Mg/B/Ti/HIT wires

The stress–strain characteristics of swaged composite wires before and after heat treatment at 635 °C/15 min were tested at low temperatures 77 K and 4.2 K, respectively. Figure 5 compares these characteristics and the highest applicable stress is shown for the swD wire in an AD state and also in a HT state. While the softest behavior is observed for the AD wire swB, this wire is stronger than swC after annealing at 635 °C. This can possibly be attributed to a positive effect of the created intermetallic Al_3Ti layer at the Ti/HIT interface as shown in figure 6. While the thickness of the Al_3Ti layer is $\sim$2 μm, in wires swC and swD a much thicker ($\sim$20 μm) layer was observed at the interface of swB made of the higher purity Al powder.

The creation of the Al_3Ti intermetallic phase at Ti/Al and its properties have been already published [27, 28]. Lu *et al* estimated a Young's modulus of Al_3Ti $E = 156$ GPa and a fracture stress to 162 MPa. This means that the Al_3Ti layer can act as reinforcing component in swB, see figure 5. The data of the microhardness of HV0.05 estimated for all the composite elements of wires swB–swD are summarized in table 3. As one can see, Ti is the hardest metal in the AD state (HV0.05 $\approx$ 250), which is reduced to around 160 after annealing. The microhardness of the MgB_2 layer (HV0.05 $\sim$ 1200) and Al_3Ti phase (HV0.05 $\sim$ 370) are nearly the same for all wires.

Figure 7 shows nano-hardness profiles across the selected part of rolled wires rwB–rwD HT at 640 °C/60 min. Similar to the case of the microhardness of the swaged wires (see table 3), the lowest hardness was measured for rwB and the largest one for rwD. No apparent differences could be observed for the hardnesses of the Ti barriers and MgB_2 in this plot, but the thickest Al_3Ti layer ($\sim$40 μm) is well visible for the rwB made of high purity Al powder in comparison to $\sim$10 μm observed in rwD. High scattering of measured values in both reactive layers (Al_3Ti and MgB_2) does not allow us to debate the sheath effect on the the superconducting phase.

3.3. Superconducting properties of MgB_2/Ti/HIT wires

The critical currents of the groove rolled wires HT at 640 °C/60 min and the rotary swaged ones annealed at 635 °C/15 min were measured at 4.2 K. Figure 8(a) shows lower engineering current densities for the rolled wires with the typical value of 10^4 Acm^{-2} measured between 4.2 and 5.5 T. The engineering current densities of the swaged wires (see figure 8(b)) are higher and less different (10^4 Acm^{-2} between 5.45 and 5.9 T), which can be attributed to a more dense and uniform boron layer prior to the final heat treatment. Nearly the same engineering current densities were measured for similarly made single-core IMD wires using the same boron powder but different metallic components MgB_2/V/Cu [29] and MgB_2/Ti/Cu [30].

This indicates well densified boron powder deformed inside the HIT sheath. Surprisingly, the strongest wires (swD or rwD) have the lowest current density and the softer ones shows better performance, which is not yet understood.

The thermal stability of the rolled and swaged wires was evaluated through the *I*–*V* curves measured far above the critical current criterion with the constant current ramping of 0.43 As^{-1} as shown in figure 9(a). The values of the power at quench and expelling of the current from the superconductor were estimated. 'Quench power density' was estimated by multiplying the current (I_q) with the voltage (V_q) and dividing it by the surface of the sample between the potential taps. Figure 9(b) presents a plot of the quench power densities versus the external field for the swaged and rolled wires with different outer sheaths. It is apparent that the swaged wires are more stable than the rolled ones, which can be ascribed to the thinner Al_3Ti interface layer (2–20 μm) at 635 °C/15 min. Doubled Al_3Ti layer thicknesses (4–40 μm) have been observed in rolled wires HT at 640 °C/60 min. The lowest quench power densities are evident for the swD and rwD wires having the most resistive and less conductive HIT, see figure 1. On the other hand, application of a more conductive outer sheath for wires swB and rwB resulted in the best stable behavior at 4.2 K, especially below 5 T where the values of the critical currents are above 200 A.

Figure 10 shows the strain and stress tolerances for the swaged wires differing only by the outer sheath. In spite of the lowest sheath hardness measured for swB (see table 3), this wire is more tolerant to axial strain than swC, see

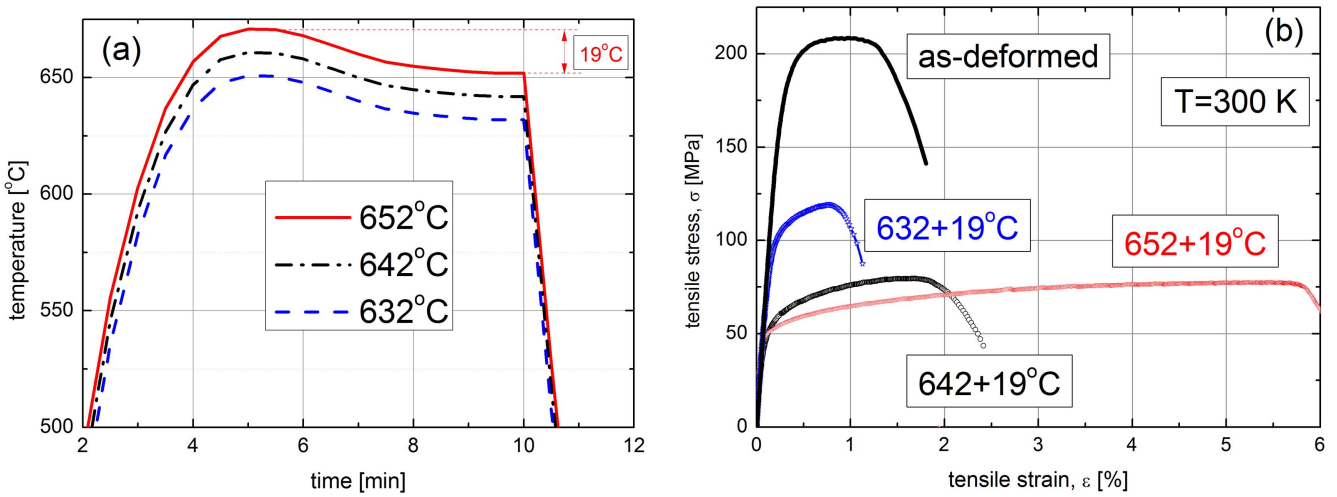

Figure 4. HT profiles applied for HIT wire wB (a) and corresponding stress–strain characteristics measured at room temperature (b).

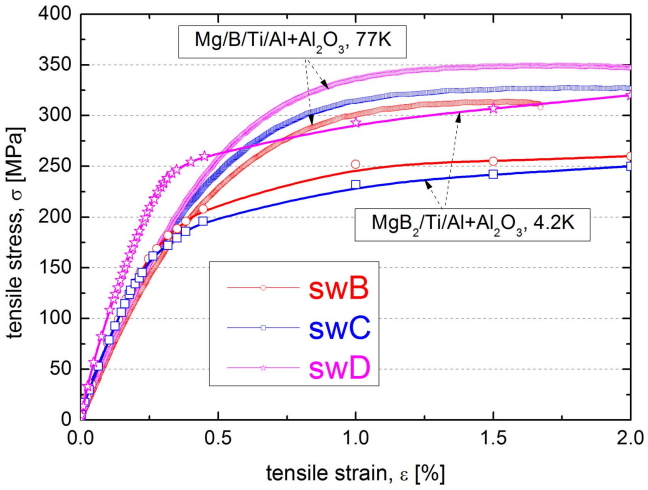

Figure 5. Stress–strain characteristics of the AD wires swB, swC, and swD at 77 K and after heat treatment at 635 °C/15 min tested at 4.2 K.

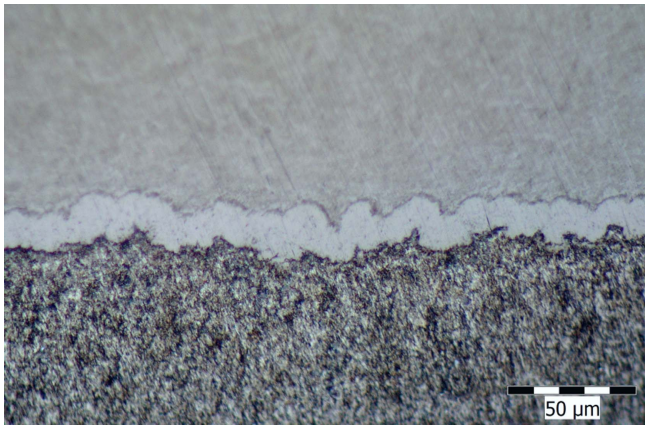

Figure 6. Picture of the Al_3Ti interface layer created in composite wire swB during the heat treatment at 635 °C/15 min.

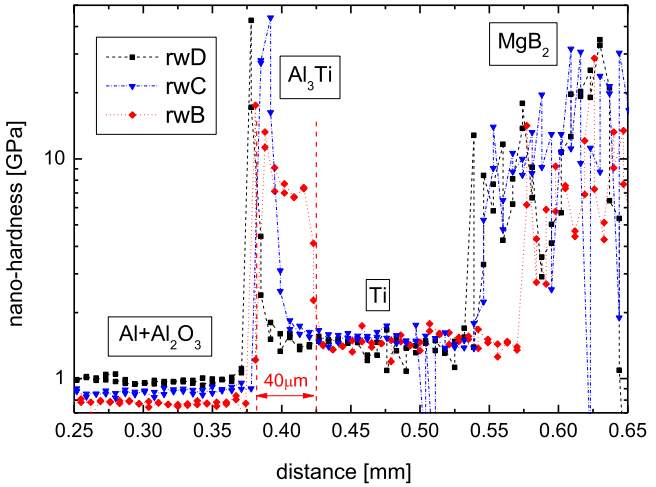

Figure 7. Nano-hardness measured across the rolled wires rwB–rwD HT at 640 °C/60 min.

Table 3. Hardness HV0.05 of composite elements before and after final heat treatment of HIT sheathed composite wires swB–swD, AD—as-deformed, HT—heat treated.

AD	swB	swC	swD
HV Al (MPa)	56	63	83
HV Ti (MPa)	252	263	230
HV Mg (MPa)	51	44	51
HT	**swB**	**swC**	**swD**
HV Al (MPa)	51	56	78
HV Ti (MPa)	164	140	173
$HVMgB_2$ (MPa)	1290	1200	1210
$HVAl_3Ti$ (MPa)	~370	~370	~370

figure 10(a). In addition, a less gradual degradation of the critical current is observed for swB above the irreversible strain limit $\varepsilon_{irr} > 0.195\%$.

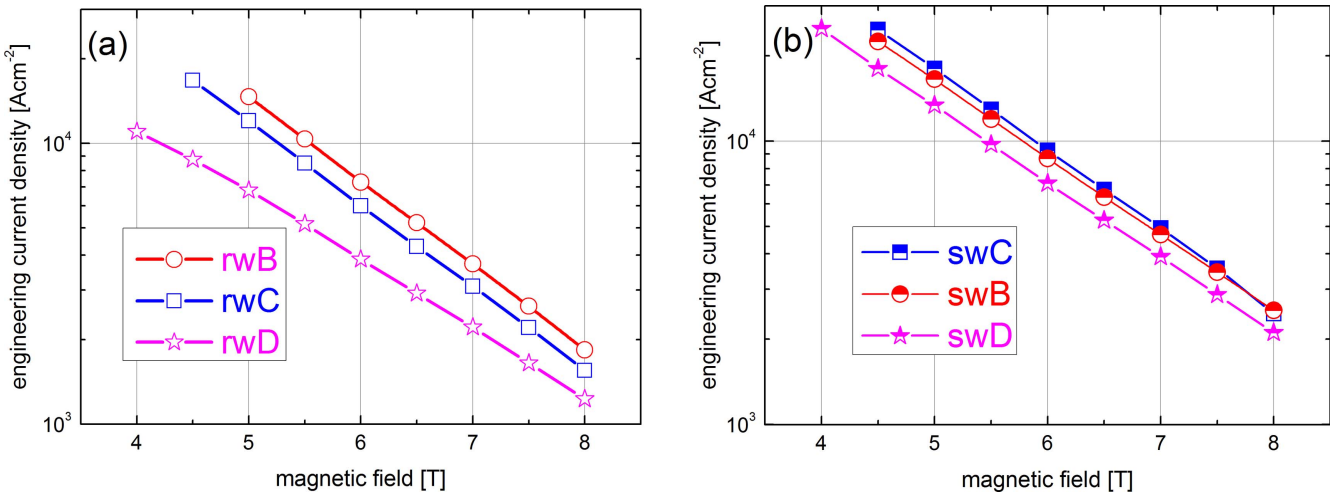

Figure 8. Engineering current densities of rolled wires HT at 640 °C/60 min (a) and swaged ones HT at 635 °C/15 min (b).

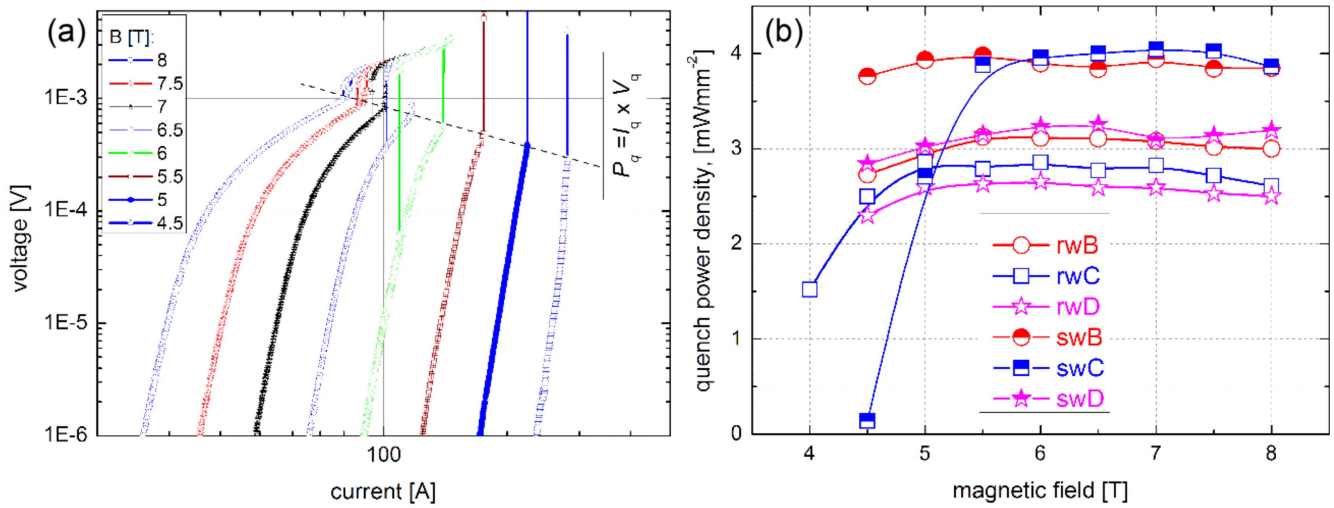

Figure 9. *I–V* characteristics of the swB wire measured at external magnetic fields between 4.5 and 8 T (a) and quench power densities versus the external field of the swaged and rolled wires (b).

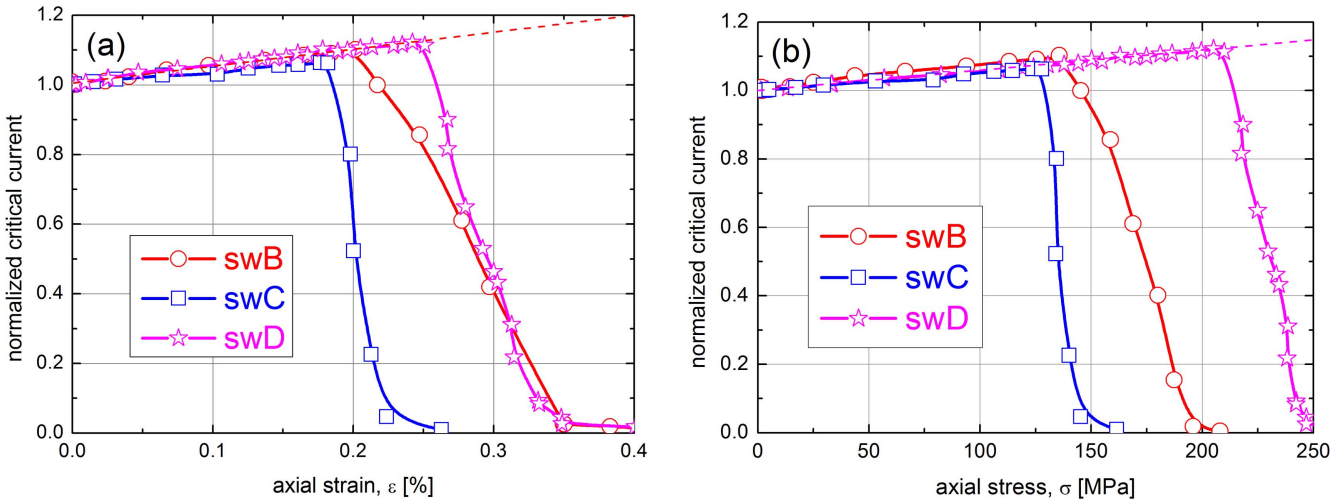

Figure 10. Critical currents of swaged wires versus axial strain (a) and tensile stress (b).

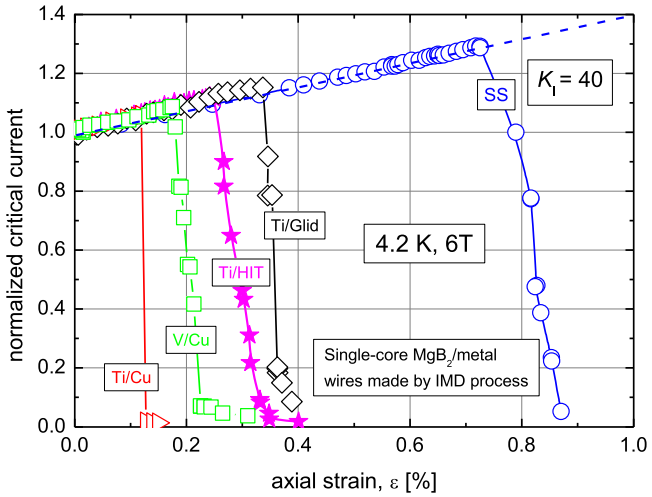

Figure 11. Strain tolerances of single-core MgB_2 wires made by the IMD process differing by the metallic sheath materials used.

Table 4. Irreversible stresses and strains of composite wires swB–swD HT at 635 °C/15 min.

Wire	swB	swC	swD
ε_{irr} (%)	0.195	0.181	0.242
σ_{irr} (MPa)	135.6	127.7	205.5

It should be noted that some reinforcing effect of the created interface Al_3Ti layer with Young's modulus $E = 165$ GPa and a fracture stress of 162 MPa [28] could be responsible for the improved strain tolerance of the swB wire. Due to the strongest outer sheath of swD (see table 3) the best strain tolerance was found for this wire with the highest $\varepsilon_{irr} = 0.242\%$, see figure 5 and table 4. Figure 9(b) shows the effect of axial stress on critical current with the highest $\sigma_{irr} = 205.5$ MPa for swD, which is increased by 61% in comparison to swC with $\sigma_{irr} = 127.7$ MPa, see table 4. It can be concluded that the strain and stress tolerance of MgB_2 wire with a HIT sheath can be adapted by the selection of an initial Al powder quality according to a requested application.

Figure 11 compares the strain tolerances ($I_c(\varepsilon)$) of single-core MgB_2 wires made by the IMD process using identical Mg wire and boron powder and differing only by the metallic sheaths. All presented $I_c(\varepsilon)$ characteristics were measured at the same conditions (4.2 K and 6 T) and with the same equipment [31]. Generally, applied axial tension partially compensates (or relaxes) the pressured MgB_2 cooled inside more contacted metallic sheath. Consequently, I_c increases up to a level of irreversible strain (ε_{irr}) where the breaking of brittle MgB_2 leads to a radical degradation. The ε_{irr} value defines the maximum strain at which the current still remains reversible [31]. Due to the undoped MgB_2 and identical conditions (6 T and 4.2 K) the slope of $I_c(\varepsilon)$ in the reversible part is nearly the same and characterized by $K_I = 40$. K_I and simply expresses the percentage increase of I_c for the eventual strain $\varepsilon = 1\%$. One can see the lowest strain tolerances for the copper sheathed wires where some positive effect of a mechanically stronger V-barrier [29] in comparison to a Ti barrier softened by the final annealing [17] is visible. Wire with a Ti barrier and GlidCop sheath [26] shows better performance ($\varepsilon_{irr} = 0.33\%$) than swD wire (named as Ti/HIT, plotted by filled stars). The best strain tolerance of MgB_2 can be obtained by a strong outer sheath, which is shown by the $I_c(\varepsilon)$ of the no-barrier wire with a stainless sheath (see blue circles in figure 11) with irreversible strain $\varepsilon_{irr} = 0.72\%$. It should be mentioned that the strain tolerances of the MgB_2 wire with a HIT sheath can be further increased by filamentary composition and/or by increased content of Al_2O_3.

4. Conclusions

Lightweight MgB_2 wires with a Ti barrier and stabilized by three kinds of $Al + Al_2O_3$ metal matrix composites were fabricated by an internal magnesium diffusion process. It was shown that the electrical, thermal, and mechanical properties of the sheaths used affect the critical current, thermal stability, and also the strain tolerance of MgB_2/Ti/HIT wires. While the HIT made of high purity Al powder offers higher thermal and electrical conductivity resulting in better thermal stability, it reacts more with the Ti barrier and creates relatively thick Al_3Ti layers (20–40 μm) during the final heat treatment. HIT sheath made of low purity Al powder is mechanically stronger, which allows for a more strain tolerant MgB_2 wire with thinner reacting layers (2–4 μm), but the thermal stability is worsened due to the lowered conductivity. Nevertheless, the presented MgB_2/Ti/HIT wire configurations are promising for lightweight, stabile, and strain tolerant superconducting wires.

Acknowledgments

This work was supported by the Slovak Scientific Agency under the APVV-14-0522 and VEGA 2/0025/14 projects. The authors are grateful to Mrs B Bartusch from IFW for the DSC measurements.

ORCID iDs

P Kováč https://orcid.org/0000-0003-1872-0359

References

[1] Zhou S, Pan A V, Ionescu M, Liu H and Dou S 2002 *Supercond. Sci. Technol.* **15** 236–40
[2] Schlachter S I, Frank A, Ringsdorf B, Orschulko H, Obst B, Liu B and Goldacker W 2006 *Physica* C **445–448** 777
[3] Kováč P, Hušek I, Melišek T, Kulich M and Štrbík V 2006 *Supercond. Sci. Technol.* **19** 600–5
[4] Kováč P, Hušek I, Dobročka E, Melišek T, Herrmann M and Haessler W 2008 *Supercond. Sci. Technol.* **21** 015004
[5] Kitaguchi H and Kumakura H 2005 *Supercond. Sci. Technol.* **18** S284–9

[6] Kim J H, Matsumoto A, Maeda M, Yamada Y, Wada K, Tachikawa K, Rindfleisch M, Tomsic M and Kumakura H 2010 *Physica* C **470** 1426–9
[7] Kováč P, Hušek I, Pachla W, Kulczyk M, Melišek T and Dvorak T 2011 *J. Alloys Compd.* **509** 8783
[8] Goldacker W, Schlachter S I, Zimmer S and Reiner H 2001 *Supercond. Sci. Technol.* **14** 787
[9] Kováč P, Hušek I, Melišek T, Kopera L and Reissner M 2010 *Supercond. Sci. Technol.* **23** 065010
[10] Kováč P, Hušek I, Melišek T and Kopera L 2013 *J. Supercond. Novel Magn.* **26** 2109
[11] Giunchi G 2003 *Int. J. Mod. Phys.* B **17** 453
[12] Giunchi G, Ripamonti G, Perini E, Ginocchio S, Bassani E and Cavallin T 2006 *Adv. Sci. Technol.* **47** 7
[13] Togano K, Hur J, Matsumoto A and Kumakura H 2010 *Supercond. Sci. Technol.* **23** 085002
[14] Li G Z, Sumption M D, Zwayer J B, Susner M A, Rindfleisch M A, Thong C J, Tomsic M J and Collings E W 2013 *Supercond. Sci. Technol.* **26** 095007
[15] Hušek I, Kováč P, Rosová A, Pachla W, Melišek T and Hain M 2014 *J. Alloys Compd.* **588** 366
[16] Ye S J, Matsumoto A, Togano K, Zhang Y C, Ohmura T and Kumakura H 2014 *Supercond. Sci. Technol.* **27** 055017
[17] Kováč P, Hušek I, Melišek T, Kopera L and Kováč J 2014 *Supercond. Sci. Technol.* **27** 065003
[18] Masson P J, Nam T, Choi T and Luongo C A 2009 *IEEE Trans. Appl. Supercond.* **19** 1662
[19] Park D H, Choi S W, Kim J H and Lee J M 2015 *Cryogenics* **68** 44
[20] Marino I, Pujana A, Sarmiento G, Sanz S, Merino J M, Tropeano M, Sun J and Canosa T 2016 *Supercond. Sci. Technol.* **29** 024005
[21] Musenich R *et al* 2016 *IEEE Trans. Appl. Supercond.* **26** 6200204
[22] Balog M, Simancik F, Walcher M, Rajner W and Poletti C 2011 *Mater. Sci. Eng.* A **529** 131–7
[23] Kováč P, Balog M, Hušek I, Kopera L, Križik P, Rosová A, Kováč J, Kulich M and Čaplovičová M 2017 *Cryogenics* **87** 58
[24] Kováč P, Hušek I, Melišek T, Kulich M, Rosová A, Kováč J, Balog M, Kopera L, Krížik P and Orovčík L 2017 *Supercond. Sci. Technol.* **30** 115001
[25] Kováč P, Hušek I, Rosova A, Kulich M, Kováč J, Melišek T, Kopera L, Balog M and Krizik P 2018 *Sci. Report* submitted
[26] Kováč P, Hušek I, Melišek T, Kopera L and Kulich M 2016 *Supercond. Sci. Technol.* **29** 10LT01
[27] Krizik P, Balog M, Nosko M, Riglos M V C, Dvorak J and Bajana B 2016 *Mater. Sci. Eng.* A **657** 6–14
[28] Lu Z, Wei N, Peng L, Guo C and Jiang F 2016 *Mater. Des.* **110** 466–74
[29] Hušek I, Kováč P, Melišek T, Kopera L, Rosová A and Szundiová B 2017 *Supercond. Sci. Technol.* **30** 105008
[30] Kováč P, Hušek I, Rosova A, Melišek T, Kulich M, Kopera L and Brunner B 2015 *Supercond. Sci. Technol.* **28** 095014
[31] Kopera L, Kováč P and Melišek T 2008 *Supercond. Sci. Technol.* **21** 115001